



High temperature transformations of the Au₇Cu₅Al₄ shape-memory alloy

Michael B. Cortie^{a,*}, Catherine S. Kealley^a, Vijay Bhatia^a, Gordon J. Thorogood^b, Margaret M. Elcombe^c, Maxim Avdeev^c

^a Institute for Nanoscale Technology, University of Technology Sydney, PO Box 123, Broadway, NSW, 2007, Australia

^b Institute of Materials Engineering, Australian Nuclear Science and Technology Organisation, PMB 1, Menai, NSW, 2234, Australia

^c Bragg Institute, Australian Nuclear Science and Technology Organisation, PMB 1, Menai, NSW, 2234, Australia

ARTICLE INFO

Article history:

Received 4 October 2010

Received in revised form 9 December 2010

Accepted 9 December 2010

Available online 16 December 2010

Keywords:

X-ray diffraction

Shape memory

Order-disorder effect

Intermetallic

Crystal structure

ABSTRACT

The β -phase of Au₇Cu₅Al₄ undergoes a reversible shape-memory phase transformation, however there has been some uncertainty regarding the crystal structure or structures of the parent phase. Here we show that, under equilibrium conditions, the parent phase possesses the L2₁ structure between its A_p (about 79 °C) and ~630 °C, and the B2 primitive cubic structure between ~630 °C and its melting point. It melts directly from B2 into the liquid state and hence never achieves the random bcc A2 structure that has been previously mooted. Splat-cast samples of the alloy are martensitic, proving that development of equilibrium order and defect concentration are not pre-requisites for the A → M transformation to occur.

© 2010 Elsevier B.V. All rights reserved.

1. Introduction

Although Al, Au and Cu each have the face-centered cubic (fcc) structure, they do not readily alloy with one another. The systems Al–Au and Al–Cu contain a series of intermetallic compounds, and while Au and Cu do form a continuous solid solution at elevated temperatures, this transforms to a series of ordered superstructures at lower temperatures. In the ternary Al–Au–Cu system two electron compounds, γ -phase Au_xCu_{9-x}Al₄ (0 < x < ~6.5) and β -phase Au_xCu_{12-x}Al₄ (0 < x < ~7.5) are known [1–3]. The 18 carat version of the β -phase, corresponding approximately to the stoichiometry Au₇Cu₅Al₄, is a shape-memory alloy (SMA) sometimes called ‘Spangold’ [4,5]. It is one of a family of precious metal SMAs that include AuCd [6], Au₂CuZn [7], TiPt [8], Au₇Cu₇Al₂ [8,9] and NiTiAu [10]. Like other SMAs, Au₇Cu₅Al₄ undergoes a reversible, displacive, thermo-elastic phase transformation between a parent (high temperature) phase and a martensitic (low temperature phase). The martensite start (*M*_s) and austenite start (*A*_s) temperatures in this alloy are normally in the range 20–30 °C and 55–80 °C respectively, with some variability due to the effect of thermal history [11,12].

The crystal structures of the parent and martensite phases are an important aspect of shape-memory alloy technology, since they influence the nature of the phase transformation and the

usable amount of strain. Although the high temperature phase of Au₇Cu₅Al₄ was initially misidentified as being similar to the L1₀ phase formed from (Au,Cu) [4,13], it was later shown that it is a Hume–Rothery β -electron compound [14]. However, it is clear that this parent phase can exist in more than one condition. For example, samples of Au₇Cu₅Al₄ aged between 100 and ~150 °C have a well-developed shape-memory effect (as evidenced by significant transformation enthalpy, surface upheaval, dilatometric signal and acoustic emission), whereas samples produced by quenching from above 450 °C do not [11,14–17]. X-ray diffraction showed that the strongly transforming samples possessed a parent phase with L2₁ ordering [14]—a condition that we will designate here as “fully aged” — but samples that have been quenched from elevated temperatures — a condition that we will designate here as “beta quenched” — have been reported to have the B2 structure [15] or mixtures of ordered phases of a nature intermediate between the A2, B2, L2₁ or DO₃ types [11,14,15,18]. Finally, metastable structures are reportedly formed when “beta-quenched” material is re-heated [18].

A schematic illustration of the A2, B2, DO₃ and L2₁ structures is provided in Fig. 1, in which it can be seen that all are variations of a body-centered cubic ABC₂ type packing. For the A2 structure the site occupancies of C are the same as those of A and B (i.e. A = B = C), for the B2 (A = B) ≠ C while for the DO₃ (A = C) ≠ B. In the L2₁ structure A ≠ B ≠ C. In general, one of the ordering sequences A2 → B2 → L2₁, A2 → DO₃, A2 → B2 → DO₃ or A2 → L2₁ is expected to occur with decreasing temperature in coinage metal β -phase

* Corresponding author. Tel.: +61 2 9514 2208.

E-mail address: michael.cortie@uts.edu.au (M.B. Cortie).

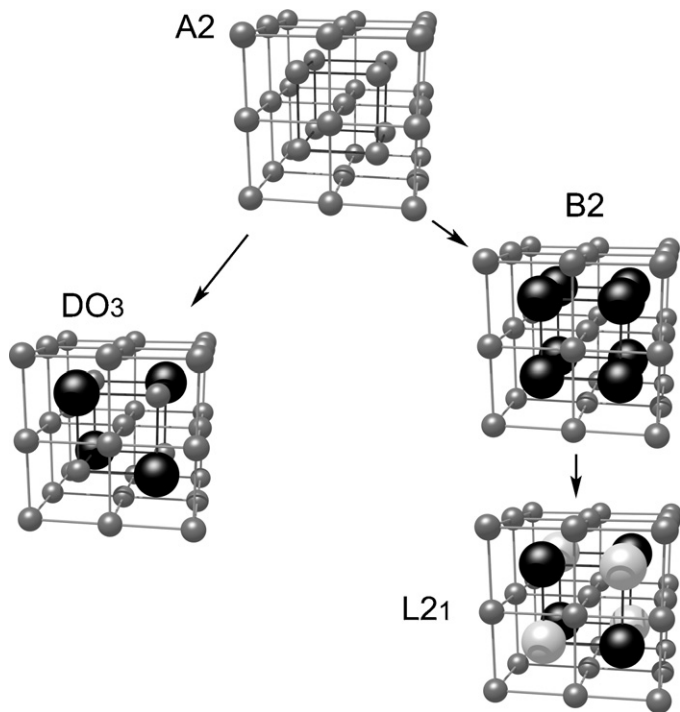


Fig. 1. Chemical ordering of the A2, B2, L₂₁ and DO₃ structures. The atoms in each case are packed in a body-centered cubic fashion but symmetries differ. All sites are equivalent in A2, which is body-centered cubic. Further ordering of A2 can produce DO₃ or B2 structures, by either first- or second-order processes. DO₃ has face-centered cubic symmetry whereas B2 can be considered to be made up of two interpenetrating simple cubic lattices. Further ordering of B2 to L₂₁ phase is possible in ternary systems by a second-order (homogenous) process, however conversion of DO₃ to L₂₁ or vice versa would normally be expected to be a first order or heterogeneous transformation.

alloys [19–21]. However, in some systems, such as AuZn or AuMn, there is no A2 and the alloy solidifies directly into the B2 structure [22,23]. The existence or absence of the A2 structure in other alloys is related to stoichiometry; for example, stoichiometric AuAgCd₂ is reported to go through the sequence L₂₁ → B2 → A2 on heating, but in off-stoichiometric compositions there is no A2 phase and instead B2 is stable to the melting point [24].

In Au₇Cu₅Al₄, differential scanning calorimetry (DSC) indicates a phase change at about 630 °C [14–16,25]. It has been generally suggested [14] or assumed [15,16,25] that the structure of the β phase above 630 °C is A2, although no direct evidence of this has been hitherto provided. There is also uncertainty whether the transformation at 630 °C is first-order [25] or second-order [15,16]. If indeed it is the A2 ↔ B2 transition occurring at ~630 °C then the B2 ↔ L₂₁ transition must necessarily occur at some lower temperature since the alloy is certainly L₂₁ ordered at 100 °C [14]. Battezzatti et al. could find no evidence for the formation or dissolution of L₂₁ and concluded that it was of a gradual, second-order nature and not readily detectable by DSC. On the other hand, they concluded that material quenched from 630 °C had the B2 structure and would transform exothermically and irreversibly to L₂₁ at 130 °C during the first reheat cycle [15]. Similarly, Gu et al. found inflections between 290 and 430 °C on cooling curves, which they attributed to the B2 → L₂₁ transition [16,25].

The structure of “beta-quenched” samples presents a further difficulty. It is known that if the ordering temperature of a non-ferrous alloy (e.g. Cu–Al–Mn) is sufficiently high, for example above 500 °C, then not even quenching can suppress subsequent binary or ternary ordering [26]. However, it is not expected in these cases that the ordering would reach the equilibrium state. In support of this, it is noted that many SMAs that have been freshly beta-quenched

either do not transform to martensite, or transform weakly or differently in comparison to samples that have been well aged (e.g. [27–29]). The suppression of the transformation may be due in some instances to the effect of quenched-in vacancies or in others to the necessity for some minimum degree of ordering to be present.

Jin et al. examined Au₇Cu₅Al₄ quenched from 680 °C and concluded [18] that it ordered to DO₃ rather than L₂₁ when re-heated up through the range 172–281 °C. A depression of the M_s from about 0 °C to –35 °C was attributed to the presence of this DO₃ parent. The structure above 630 °C was believed to be A2. Battezzatti et al. [15] showed that when Au₇Cu₅Al₄ was rapidly solidified onto a copper wheel, and not allowed to cool below 17 °C, it consisted of a partially transformed mixture of L₂₁ phase and martensite. It transformed back to parent phase on heating with an enthalpy of only 1.1 J/g (compared to the usual 3 to 3.5 J/g [15,30]). The lower enthalpy was attributed to the lower volume fraction of martensite present. However, a sample that had been beta quenched from 630 °C appeared to consist of only the B2 phase.

Clearly, the structure of the β-phase at higher temperatures, and the results produced by quenching it, have remained uncertain. Here we have used *in situ* X-ray and neutron powder diffraction studies to resolve these uncertainties.

2. Material and methods

The samples for this project were manufactured using high purity base metals of Au (99.99%), Cu (99.9%) and Al (99.99%) melted in an alumina crucible under a protective layer of carbon pellets. The Au was melted first, and then the Cu and Al stirred in. The samples were annealed at 700 °C to convert them into β-phase, followed by quenching into iced brine. Gravity splat-cast samples (GSC1) were produced by either being poured in the molten state onto a cold refractory plate (GSC1) or onto a copper plate (GSC2), whereas impact splat cast (ISC1 and ISC2) samples were made by dropping a copper block onto a molten bead of the alloy. Samples GSC1, GSC2 and ISC1 were peeled off their respective substrates and not cooled below –5 °C prior to analysis. In contrast, sample ISC2 was immediately stored into liquid nitrogen after solidification but then reheated to room temperature 3 h later for X-ray diffraction.

DSC analyses were performed using a Thermal Analysis DSC 2920 with a ramp rate of 10 °C/min. Samples were also pulverized in a ring-mill for diffraction studies, and annealed at 500 °C for 1–3 h to remove strain. Mössbauer spectroscopy was performed at 4 K using an activated Au source and a transmission configuration.

Powder diffraction was undertaken at the Australian Synchrotron (10BM1: Powder Diffraction) on spinning 0.3 and 0.5 mm capillaries filled with Au₇Cu₅Al₄ powder between room temperature and 800 °C. Synchrotron data were collected from a LaB₆ Standard (NIST 660a) to accurately calibrate the wavelength and determine the instrument contributions to the observed line profiles. Samples were analyzed at an incident wavelength of 1.12715 ± 0.00001 Å (0.5 mm capillary) and 1.15970 ± 0.00001 Å (0.3 mm capillary) as these provided the best peak shape and peak-to-background ratio within the available energy range of the instrument. X-ray patterns of bulk samples were obtained on laboratory machines using either Cu Kα or Mo Kα radiation. Due to the large grain size of the material, the patterns of the bulk samples were strongly effected by texture.

While the overall structure is already known to be based on body-centered cubic packing, determination of the site occupancies is crucial to determine the actual crystal structure type. The X-ray patterns are dominated by the scattering length of the Au component. Hence, in order to resolve the site occupancies, complementary neutron powder diffraction data were collected on Echidna (the high resolution powder diffractometer) at the OPAL reactor at ANSTO in Australia because neutron diffraction is more sensitive to the Al positions in this system (see later). Data were collected from stationary powder samples at 200, 550 and 700 °C using a neutron wavelength of 1.5388 Å.

An estimate of the lattice occupancy was made using a Pascal script running within Crystallographica¹ that iterated through the permutations of occupancy of Au, Al and Cu on the A, B and C sites of a notional ABC₂ Heusler-type arrangement adjusted for the actual stoichiometry of Au₇Cu₅Al₄. The suitability of a permutation was judged by calculating the ratios of selected superlattice and fundamental peaks on the patterns. In particular, the {1 1 1} peak, which is generated by ternary ordering of the L₂₁ or DO₃ types, was assessed relative to the fundamental body centered cubic {2 0 0} and {4 2 2} peaks, while the {2 0 0} and {4 2 0} peaks, which

¹ Crystallographica is a product of Oxford Cryosystems Ltd, of 3 Blenheim Office Park, Lower Rd, Long Hanborough, Oxford OX8 8LN, UK.

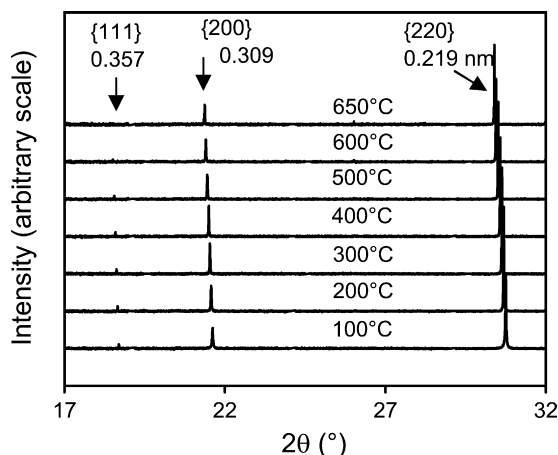


Fig. 2. Portion of synchrotron X-ray diffraction pattern, with scans taken over a range of temperatures, showing the presence of the {1 1 1} and {2 0 0} peaks associated respectively with ordering of the ternary (L_{21}) and binary (B2) types, and the fundamental {2 2 0} peak associated with the underlying body-centered cubic lattice. The peak positions in nm are for the 100 °C data.

are generated by binary ordering of the B2 type [14], were assessed relative to the {2 2 0} and {4 2 2} respectively. Use of more than one peak to estimate the ordering provided a means of reducing the effects of any texturing (preferred orientation) in the sample. The algorithm used (see Supporting Data for the script) searched for the minimum value of the parameter, s :

$$s = \left(\frac{I_{111}}{I_{220}} - \frac{I_{111M}}{I_{220M}} \right)^2 + \left(\frac{I_{111}}{I_{422}} - \frac{I_{111M}}{I_{422M}} \right)^2 + \left(\frac{I_{200}}{I_{220}} - \frac{I_{200M}}{I_{220M}} \right)^2 + \left(\frac{I_{420}}{I_{422}} - \frac{I_{420M}}{I_{422M}} \right)^2$$

where I_{xxx} is the calculated height of the indicated peak, and I_{xxxM} is the measured area of that peak. The effect of thermal vibration was ignored. The calculation was repeated for both X-ray and neutron data and the average value of s for the two radiations used to drive the optimization using the method of steepest descent.

3. Results and discussion

3.1. Absence of the A2 structure

During heating from low temperatures, the martensite of $Au_7Cu_5Al_4$ transforms into the high temperature parent phase by a displacive, first-order phase transformation. The transition occurs between 55 and 85 °C, depending on prior thermal history [11]. The martensite has a relatively complex crystal structure, which is easily recognizable on the diffraction patterns, but we will not discuss it further here.

A series of parent phase diffraction patterns at temperatures from 100 °C upwards is shown in Fig. 2. The {2 2 0} peak is one of the fundamental peaks of the underlying body-centered cubic lattice and is always present, whereas the presence of a well-developed {2 0 0} peak indicates that binary ordering of the B2 type has occurred. The {1 1 1} peak is visible on patterns taken from 100 °C to about 600 °C, but is always considerably lower in height here than the {2 0 0}. In general, the presence of the {1 1 1} and {3 1 1} peaks indicates either binary DO_3 or ternary L_{21} ordering, but the relationship of peak heights in the present case ($I_{220M} \gg I_{111M}$) shows that the ordering must be of the L_{21} type [14].

Fig. 3 shows the sum of the peak areas of the first three fundamental bcc A2 reflections ({2 2 0}, {4 0 0} and {4 2 2}), the sum of the first three B2 reflections ({2 0 0}, {2 2 2} and {4 2 0}) and the sum of the first two reflections due to ternary ordering ({1 1 1} and {3 1 1}) plotted from 300 to 800 °C. Summing the peaks in this way helps reduce effects due to crystallographic texture in the sample. Loss of the L_{21} ordering on heating through about 620 °C is evident. The transition starts at temperature a and ends at b . Melting of the material is indicated by the drastic decline in peak intensity between temperatures s and l , corresponding to solidus and

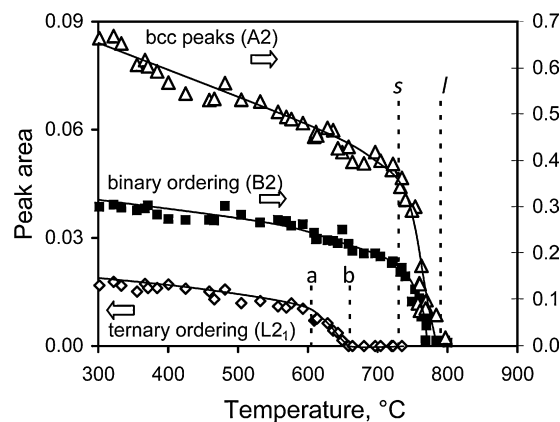


Fig. 3. Effect of temperature on diffraction peaks caused by ternary, binary and no ordering (0.5 mm capillary). Trend lines are merely to guide the eye. Relevant vertical axes for data sets indicated by arrows. It is clear that the L_{21} phase transforms to B2 between points a and b and that the sample melts between solidus (s) and liquidus (l).

liquidus respectively. It is important to note that the peaks due to B2 ordering retain their intensity up to the liquidus. The overall decrease in peak intensity with increase in temperature in Fig. 3 is due to increase in thermal vibration. It is clear from these plots that the material is L_{21} -ordered from the A_5 up to about 620 °C, and B2-ordered from about 620 °C to the melting point. The recent reports [15,16,25] in the literature of the existence of the A2 structure or of various phase transformations from A2 to L_{21} or DO_3 need to be re-visited in the light of these results.

3.2. Lattice occupancies and cell parameters

The overall pattern of the parent phase between 80 and 630 °C can be indexed as a face-centered cubic structure, with the space group $Fm\bar{3}m$. However, examination of the effect of possible permutations on occupancy on the calculated diffraction pattern showed that the X-ray pattern could, in principle, be generated by more than one arrangement of atoms (Fig. S1a, Supporting Information), whereas simulations made using neutron radiation indicated a single, but extended, range of possibilities (Fig. S1b, Supporting Information). Fortunately, consideration of the X-ray and neutron data *simultaneously* shows that the only possible common solution has an Au occupancy on the C site of about 0.8 and an Au occupancy on the B site of nearly zero (Fig. S1c, Supporting Information). In both cases, the Al of this common solution is found to be concentrated on the B site. The details of the X-ray pattern are most sensitive to the location of the Au atoms, Fig. 4, as the atomic number of Au (79) is considerably greater than that of Al (13) or Cu (29). In contrast, optimization of occupancy against the neutron pattern was not very sensitive to the Au and Cu occupancies because they have rather similar neutron scattering cross-sections (7.32 vs. 7.49 barns respectively). In this case it was more useful to optimize the structure with respect to Al content (because the coherent scattering cross section of that element (1.50 barns) is quite different to Au or Cu. The best solution (Fig. S2a and c, Supporting Information) has an Al occupancy of about 0.90–0.95 in the B site and negligible amounts elsewhere.

The best-fitting occupancies taken by considering the X-ray and neutron data simultaneously are listed in Table 1 for data collected at 200, 550 and 700 °C. The starting guess for the steepest-descent algorithm was an Au occupancy of 0.8 in the C site and none in the B site, and 0.8 Al in the B site and none in the A site. (The other occupancies can be calculated from these values by reference to the stoichiometry of the alloy). Given that the starting patterns were influenced by some texture, we estimate that the occupancy val-

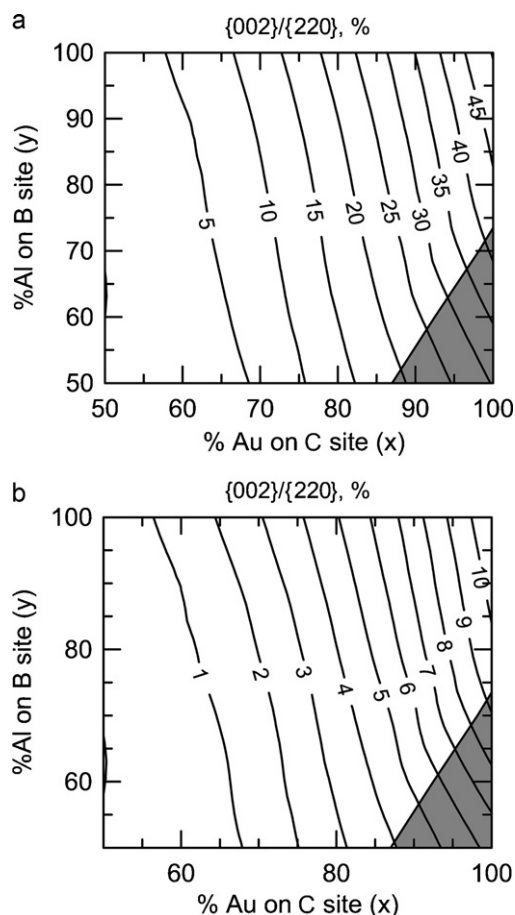


Fig. 4. Effect of distribution of Au and Al atoms on (a) ratio of $\{200\}$ peak height to $\{220\}$ peak height, (b) ratio of $\{222\}$ to $\{220\}$ peak height. The shaded regions are not possible with the stoichiometry of $\text{Au}_7\text{Cu}_5\text{Al}_4$. The Au occupancies exert a dominant effect on the X-ray diffraction pattern.

ues in the Table are not more accurate than ± 0.05 . Nevertheless, it can be seen that the lattice at 200°C has slightly better developed $L2_1$ ordering than the one at 550°C , and that the ordering on the A site decreased slightly as the temperature was varied from 200 to 700°C . The diffraction patterns calculated by this optimization method are compared to measured ones in Fig. 5 for data taken at 200°C . A similar quality of fit was obtained at other temperatures.

The synchrotron data is severely affected by absorption. Even with a 0.3 mm sample diameter the μr is ~ 6 . Working with the true

Table 1

Best-fitting solutions to lattice occupancy of $\text{Au}_7\text{Cu}_5\text{Al}_4$ β phase at various temperatures obtained by iteration over possible permutations of occupancy in *Crystallographica*. Accuracy of entries estimated to be not better than 0.05 due to residual texture effects in samples.

	Site		
	A	B	C
200 °C			
Au	0.07	0.06	0.80
Al	0.00	0.94	0.02
Cu	0.93	0.00	0.18
550 °C			
Au	0.16	0.07	0.76
Al	0.16	0.82	0.00
Cu	0.68	0.12	0.25
700 °C			
Au	0.74	0.13	–
Al	0.00	0.48	–
Cu	0.26	0.39	–

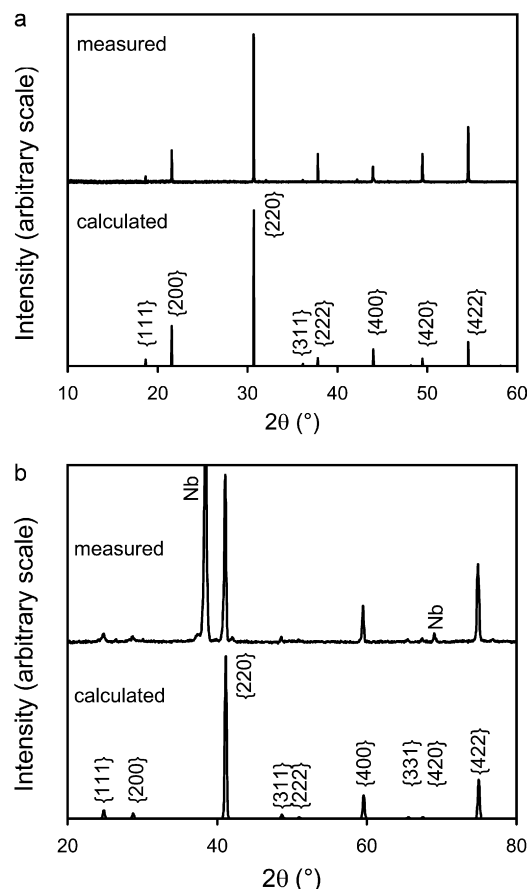


Fig. 5. Best-fitting simulations of the X-ray and neutron diffraction patterns obtained at 200°C . The neutron diffraction pattern also contains niobium peaks from the furnace.

integrals shows that this gives rise to an intensity reduction across the pattern of $\sim 99.7\%$ at 0° to $\sim 98\%$ at 90° , a peak shift (of centroid) from 0° at 0° to $\sim +.012^\circ$ at 20° reducing to $\sim +.007^\circ$ at 90° , and a reduction in the sample contribution to the peak width of $\sim 96\%$ at 20° to $\sim 70\%$ at 90° with an associated shape change to an asymmetric triangle. While various empirical approximations are available for the intensity variation and the width variation can be taken care of with adjustments to the U and W parameters, none of Rietica, GSAS or FULLPROF² have satisfactory approximations for the peak shift or shape change. As a consequence we have not yet been able to perform the final Rietveld refinements of the synchrotron data or perform joint Rietveld refinements with the neutron data. However the relative changes in lattice parameter and thermal parameters with temperature can be used to demonstrate features of the data. The Rietveld refinements will be the subject of a separate paper.

It is clear, however, that a significant phase transition occurs at 630°C , in which atoms randomize on the A and B sites, forming a primitive cubic phase, B2. An example of the refinement for the $L2_1$ and B2 materials is given in Fig. 6, for data collected at 541 and 720°C respectively. The space group of the 720°C data is $Pm\bar{3}m$, and the lattice parameter is 3.132 Å. There are two sites present in this structure, the Au-rich site ($x=0.0, y=0.0, z=0.0$), and the other site ($x=0.5, y=0.5, z=0.5$) with random ordering of the remaining elements. The odd reflections present show that the high temperature phase is primitive cubic. As mentioned, the intensity of the peaks

² RIETICA, GSAS and FULLPROF are free utilities available from <http://www.rietica.org>, <http://www.ncnr.nist.gov/xtal/software/downloads.html> and <http://www.ill.eu/sites/fullprof> respectively.

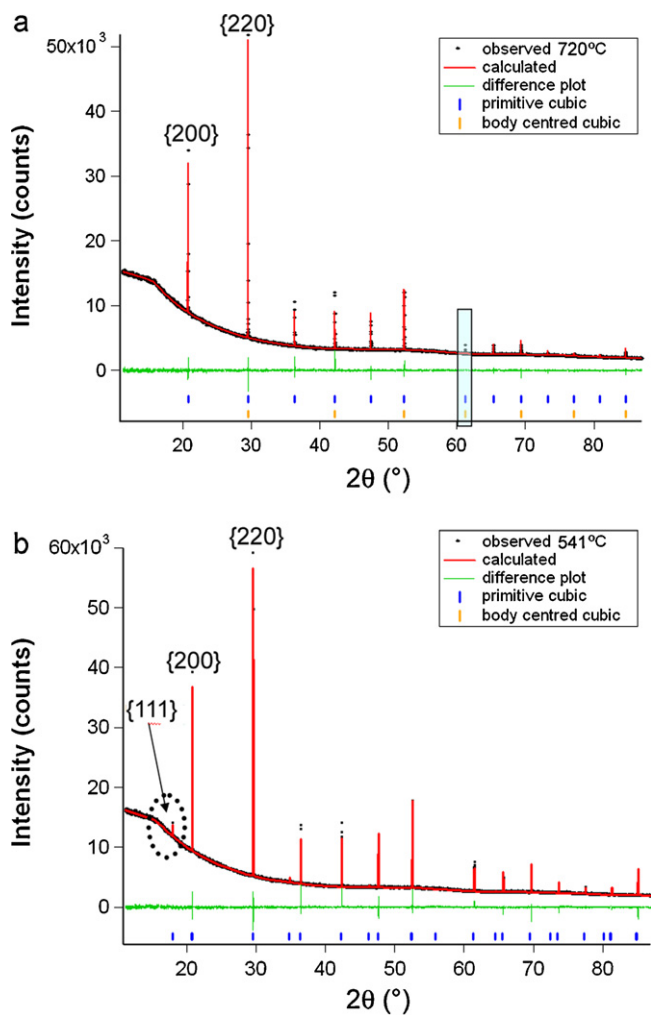


Fig. 6. Rietveld refinement of the synchrotron powder diffraction data collected at 720 °C and 541 °C (the blue box is an excluded region, as half of the reflection has fallen into the detector gap). The {200} peak of the B2 phase is clearly visible at both temperatures, while the {111} peak generated by ternary ordering is absent at 720 °C.

during a heating scan start to drop off at ~ 730 °C, indicating that melting is taken place. The B2 phase was retained through to the last vestiges of solid material to melt, disproving the assumptions made in the previous literature [15,16,25] of a high temperature A2 structure.

3.3. Removal of lattice strain

Although the powdered samples had been annealed prior to the synchrotron experiment, transformation from martensite into the parent phase generates new strain, of the order of 2–4% [31]. When this annealed out during the heating scan, there was a corresponding increase in peak height, Fig. 7 (upper curves). It is evident that the stresses were annealed out at by about 300 °C for the 220 but in some directions the height did not maximize until ~ 400 °C. The overall area under the peaks Fig. 7 (lower lines), however, only showed the expected monotonic decline due to increased thermal vibration, indicating that no change in volume fraction of the parent phase had occurred. However during the cooling scans, Fig. 7, there were increases in peak heights at different rates for different reflections which requires further explanation. Similar results were obtained for the 0.5 mm capillary.

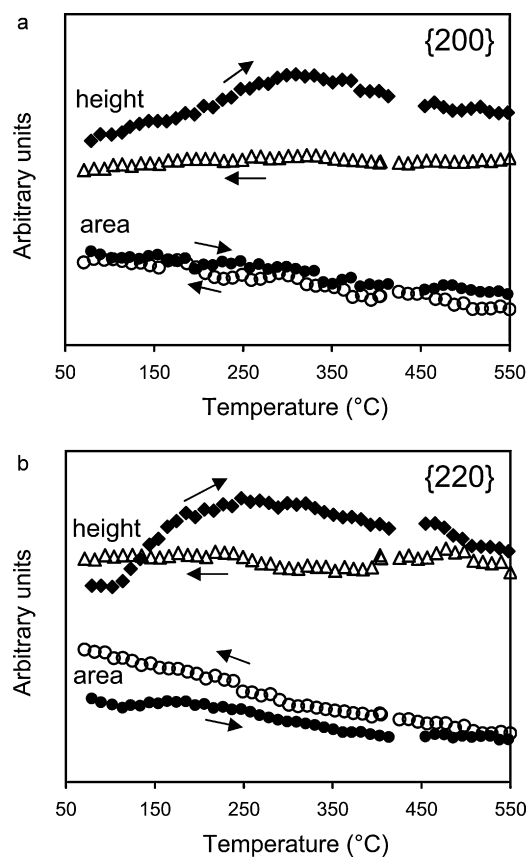


Fig. 7. Change in height and area of a) {200}, a peak generated by B2 ordering, and b) {220}, a fundamental body-centered cubic peak. In each case the heating part of the scan is associated with an increase in peak height up to about 300 °C. In contrast, the area under the peaks appears to be influenced only by thermal vibration.

3.4. B2/L₂₁ transition

The lattice parameter for the two parent phases (L₂₁ and B2) is plotted as a function of temperature in Fig. 8. It can be seen that there is a marked change in slope at ~ 630 °C, but no discontinuity,

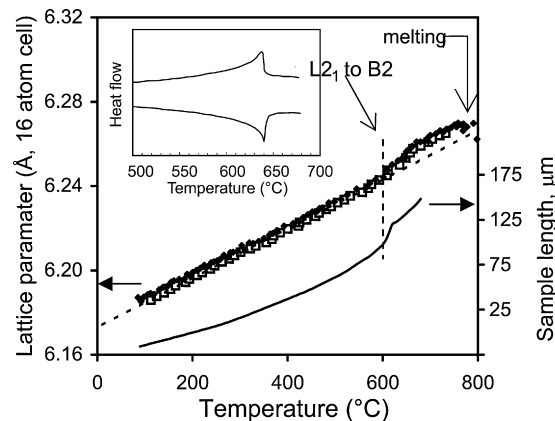


Fig. 8. Lattice parameter as a function of temperature determined from a refinement of the synchrotron data (hollow squares) and independently from the peak positions using the expression $a = d_{hkl} \sqrt{(h^2 + k^2 + l^2)}$ (closed diamond symbols) (note: B2 primitive cell value doubled for ease of plotting). Also shown is the thermal contraction data of Jin et al., obtained by digitizing their Fig. 1 [25]. There is a change in the lattice parameter and sample length at 630 °C, corresponding to the L₂₁ ↔ B2 transformation. The forward and reverse heat flows measured in this alloy for this transformation are shown as an inset, reproduced with permission from Levey et al. [17]. The thermal signal shows the classic shape of a second-order phase transformation [19].

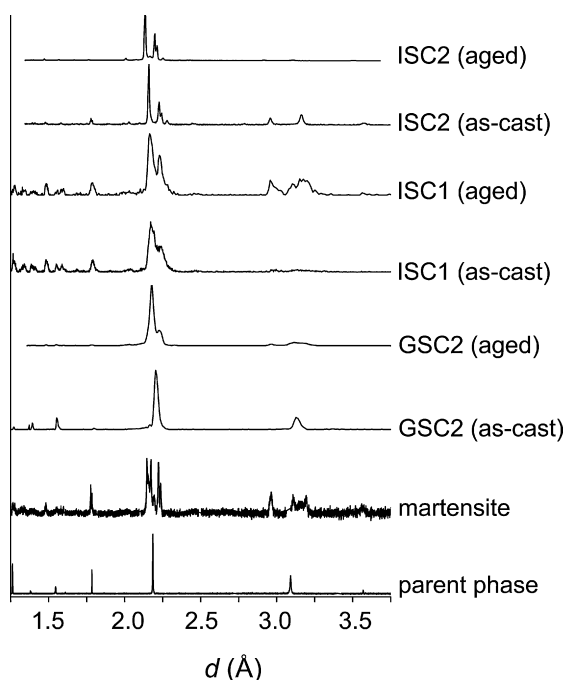


Fig. 9. X-ray diffraction patterns of three splat-cast samples and two standard samples, showing that most of the splat-cast samples were martensitic. The exception is sample GSC2, which appears to have been substantially comprised of B2 phase immediately after solidification. Different radiations have been used, so the data have been plotted against interplanar spacing, d , for the purposes of comparison. (The radiations used were: ISC2 – Cu $K\alpha$, ISC1 – Mo $K\alpha$, GSC2 – Cu $K\alpha$, typical martensite – synchrotron 1.12715 Å, typical parent phase – synchrotron 1.53878 Å.

factors which taken together with the DSC data (λ shape of curve and lack of undercooling, inset to Fig. 8) tend to indicate that this is a second-order transition, cf. Obrado et al. [19] and Battezzati [15]. The trends in the lattice parameter data match those of the thermal contraction data of Jin et al. [25], which are also shown on Fig. 8.

3.5. Structure of beta-quenched material

As we have shown here, solid $Au_7Cu_5Al_4$ has the B2 structure at temperatures above 630 °C so any transitions observed in beta quenched material must begin from the B2 phase. Therefore, the transformation observed by Jin et al. [18] could only have been a B2 \rightarrow DO₃ transition and not an A2 \rightarrow DO₃ transformation. It is reported that the A2 \rightarrow DO₃ and B2 \rightarrow DO₃ transformations are almost inevitably first-order for reasons relating to symmetry [19] so if DO₃ phase did precipitate it should be apparent in microstructural sections or diffraction patterns. The associated internal friction and electrical resistivity changes previously observed in the 200–400 °C range [16,18,25] need further investigation. However, the present results clearly show that these changes must be due to short, rather than long range ordering, since they are not shown in our X ray diffraction patterns.

The X-ray diffraction patterns of three of these samples are compared in Fig. 9 to patterns obtained in the synchrotron for ‘equilibrium’ powders of martensite and parent phase. The patterns of the splat-cast samples are of comparatively poor quality, as the newly solidified foil was placed directly onto the stage of the X-ray machine, with no other specimen preparation. The patterns would therefore be expected to show the effects of preferred orientation, surface oxides, and lack of flatness. Nevertheless, it is clear that samples ISC1 and ISC2 were martensitic at the time of their first measurement. Furthermore, there is no evidence that aging of these samples (for 72 h at room temperature, and about one

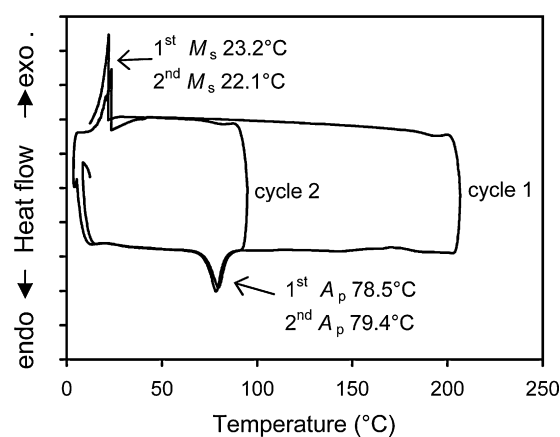


Fig. 10. Thermal analysis of splat-cast sample ISC2, after two days aging at room temperature, showing that it was fully capable of reverting to parent phase.

week at temperatures between 20 and 60 °C respectively) changed this martensite, and such differences as there are between the four patterns may be attributed to sampling and/or instrumental factors. The ISC2 sample underwent a well-developed transition to austenite when reheated, with an A_p of 79 ± 0.5 °C, and this was not changed by a subsequent heat treatment at 200 °C, Fig. 10. On the other hand the GSC2 sample appeared to have contained little martensite in the as-cast condition, but had certainly developed the characteristic split peaks of martensite after several weeks of aging at room temperature. Clearly, the splat-cast microstructure of $Au_7Cu_5Al_4$ is acutely sensitive to cooling rate, with the GSC2 sample here, and the samples of Battezzati (copper wheel) and Levey (water-cooled copper hearth), having been cooled sufficiently fast to suppress the M_s to below the temperature of the quench medium. However, it appears that there is a time-dependent process that gradually raises the M_s of such β -phase samples so that they convert to martensite at room temperature after several weeks.

Thermal analysis of a portion of sample GSC1 that had been freshly re-beta-quenched from 700 °C and quenched into iced brine [11] failed to show an A_s , indicating that the M_s was well below 0 °C when in this condition. However, after such a beta-quenched sample was aged at 150 °C then quenched again into iced brine, thermal analysis indicated an A_s at 81.5 °C. A further martensitic stabilization treatment of such material at 60 °C for 17 h resulted in an A_s of 84.6 °C. This is evidence that, provided it has received a prior aging treatment in the 140–450 °C range, $Au_7Cu_5Al_4$ is only slightly susceptible to the phenomenon of ‘martensite stabilization’.

The results of applying Mössbauer spectroscopy to the GSC1 splat-cast foil of the 5.8 wt% Al alloy after two years of aging at room temperature, and to pure gold, are listed in Table 2 and shown in Fig. 11. The absorption spectrum of the alloy displayed the same inverted Gaussian shape as for pure gold, but the minimum was shifted (the isomeric shift) by +3.21 mm/s. No quadrupole splitting was visible, implying that the gold atoms in this sample were in an approximately cubic configuration and that the gold in the sample was present in a single phase, at least to within

Table 2
Mössbauer parameters for Au and $Au_7Cu_5Al_4$.

Parameter	Au	$Au_7Cu_5Al_4$
Shape	Simple inverted Gaussian	Simple inverted Gaussian
Isomeric shift	–1.05 mm/s	+2.16 mm/s
Line width	2.60	2.52
Area	0.21	0.23

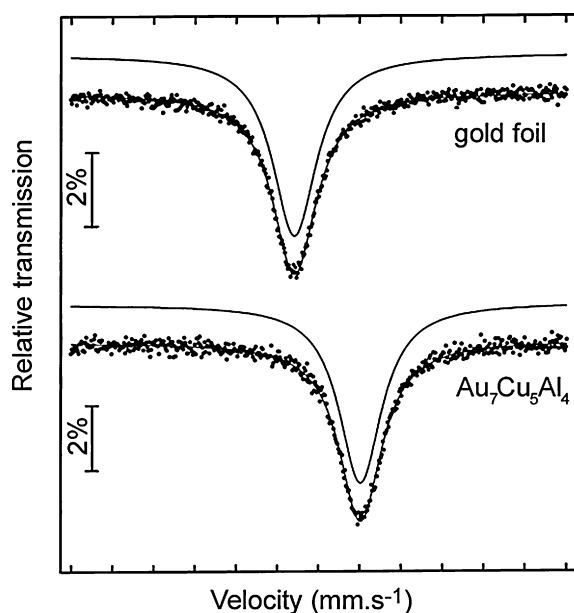


Fig. 11. Mössbauer spectra for foils of pure gold and $\text{Au}_7\text{Cu}_5\text{Al}_4$ indicating an approximately cubic symmetry for the gold atoms and a pronounced isomer shift for the alloy relative to pure gold.

the resolution of the measurements. However, the line widths for the two measurements are comparatively large (for comparison, measurements in the literature for Au and AuCd show line widths in the range 1.90–2.50 mm/s depending on microstructure [32,33]), implying that an excessive specimen thickness or some other experimentally-derived source of noise is obscuring the data in the present instance. The isomeric shift of the experimental alloy with respect to pure gold is caused by a changed electronic state of the Au atoms, due especially to the fact that their nearest neighbors are no longer all Au atoms. Since gold is noble (electronegative), the introduction of an electropositive metal into the lattice tends to decrease the electronic charge around the gold atoms, thereby causing the isomeric shift.

4. Conclusions

The $\text{Au}_7\text{Cu}_5\text{Al}_4$ alloy does not achieve the fully randomized A2 structure at any stage, in contrast to previous reports or suggestions. The highest temperature solid phase has the B2 (primitive cubic) structure. It appears that the B2 structure transforms to L2₁ on cooling through $\sim 630^\circ\text{C}$, and that this transition is second-order in nature. The lattice parameters and chemical occupancy of the parent phase have been estimated. The reversion of martensite to parent phase during a heating scan generated strain, but this effect was annealed out by about 400°C . Splat-cast samples of $\text{Au}_7\text{Cu}_5\text{Al}_4$ are martensitic if cooled below the M_s , but can be retained in the parent phase condition by keeping the minimum sample temperature above the M_s .

Acknowledgements

This research was undertaken on the powder diffraction beamline at the Australian Synchrotron, and on the Echidna neutron diffraction beamline of the OPAL reactor at the Australian Nuclear Science and Technology Organization. The authors would like to thank AINSE Ltd for providing Award No 5597. The DSC scan inset in Fig. 7 was originally kindly run by Mettler–Toledo of Switzerland and originally published in Levey et al. [17]. The Mössbauer data were provided by the late Prof. Herman Pollock of the University of Witwatersrand, Johannesburg, South Africa and his colleagues Dr. Gio Hearne and Mr. Seda Takele.

Appendix A. Supplementary data

Supplementary data associated with this article can be found in the online version, at doi:10.1016/j.jallcom.2010.12.068.

References

- [1] F.C. Levey, M.B. Cortie, L.A. Cornish, *Metall. Mater. Trans. A* 33A (2002) 987–994.
- [2] V.K. Bhatia, C.S. Kealley, A. Dowd, F.C. Levey, M.B. Cortie, *Gold Bull.* 42 (3) (2009) 201–208.
- [3] V.K. Bhatia, C.S. Kealley, R. Wuhler, K.S. Wallwork, M.B. Cortie, *J. Alloys Compd.* 488 (2010) 100–107.
- [4] I.M. Wolff, M.B. Cortie, *Gold Bull.* 27 (2) (1994) 44–54.
- [5] M. Cortie, I. Wolff, F. Levey, S. Taylor, R. Watt, R. Pretorius, T. Biggs, J. Hurly, *Gold Technol.* 14 (1994) 30–36.
- [6] L.C. Chang, T.A. Read, *Trans. AIME* 191 (1951) 47–52.
- [7] G.B. Brook, R.F. Iles, *Gold Bull.* 8 (1) (1975) 16–21.
- [8] T. Biggs, M.B. Cortie, M. Witcomb, L.A. Cornish, *Mater. Trans. A* 32A (2001) 1887–1902.
- [9] Y. Isobe, Form retaining alloy, Japanese Patent JP 2267237 (1991).
- [10] S. Besseghini, F. Passaretti, E. Villa, P. Fabbro, F. Ricciardi, *Gold Bull.* 40 (4) (2007) 328–335.
- [11] F.C. Levey, M.B. Cortie, L.A. Cornish, *Metall. Mater. Trans. A* 31 (2000) 1917–1923.
- [12] S. Urbano, A. Manca, S. Besseghini, G. Airoidi, *Scripta Mater.* 52 (4) (2005) 317–321.
- [13] H. Sato, R.S. Toth, *Phys. Rev.* 124 (6) (1961) 1833–1847.
- [14] M.B. Cortie, F.C. Levey, *Intermetallics* 8 (7) (2000) 793–804.
- [15] L. Battezzati, G. Fiore, M. Massazza, *J. Alloys Compd.* 434/435 (2007) 264–267.
- [16] Y. Gu, M. Jin, X. Jin, *Intermetallics* 17 (9) (2009) 704–709.
- [17] F.C. Levey, M.B. Cortie, L.A. Cornish, *J. Alloys Compd.* 354 (2003) 171–180.
- [18] M. Jin, J. Liu, X. Jin, *Intermetallics* 18 (5) (2010) 846–850.
- [19] E. Obrado, C. Frontera, L. Manosa, A. Planes, *Phys. Rev. B* 58 (1998) 14245.
- [20] M.H. Wu, C.M. Wayman, *Scripta Metall. Mater.* 25 (1991) 1633–1640.
- [21] T. Makita, M. Kobukata, A. Nagasawa, *J. Mater. Sci.* 21 (1986) 2212.
- [22] A. Prince, G.V. Raynor, D.S. Evans, *Phase Diagrams of Ternary Gold Alloys*, The Institute of Metals, London, 1990.
- [23] B.H. Chen, H.F. Franzen, *J. Less Comm. Metals* 143 (1988) 331.
- [24] T. Suzuki, S.I. Nakamoto, *Mater. Sci. Eng. A* 273 (1999) 549–553.
- [25] M.J. Jin, Y.J. Gu, X. Jin, *Mater. Charact.* 60 (2009) 1395–1399.
- [26] Y. Sutou, T. Omori, R. Kainuma, K. Ishida, *Mater. Sci. Technol.* 24 (8) (2008) 896–901.
- [27] J.D. Stice, C.M. Wayman, *Metall. Trans. A* 13 (1982) 1687.
- [28] R. Romero, A. Somoza, M.A. Jurado, A. Planes, L. Mañosa, *Acta Mater.* 45 (5) (1997) 2101–2107.
- [29] T. Makita, A. Nagasawa, *Scripta Metall.* 18 (1984) 1275.
- [30] L. Fumagalli, S. Besseghini, F. Passaretti, G. Airoidi, *J. Alloys Compd.* 433 (2007) 332–337.
- [31] M.B. Cortie, F.C. Levey, *Intermetallics* 10 (2002) 23–31.
- [32] J.A. Sawicki, B.D. Sawika, *Hyperfine Interact.* 16 (1–4) (1983) 1013–1016.
- [33] J.D. Cashion, J. Chadwick, C.M. Coyle, T.R. Finlayson, *J. Phys. IV France* 112 (2003) 1087–1090.